energies

MDPI

Article

A Hybrid Fault Recognition Algorithm Using Stockwell Transform and Wigner Distribution Function for Power System Network with Solar Energy Penetration

Atul Kulshrestha [1], Om Prakash Mahela [2,*], Mukesh Kumar Gupta [1], Neeraj Gupta [3], Nilesh Patel [3], Tomonobu Senjyu [4,*], Mir Sayed Shah Danish [4] and Mahdi Khosravy [5,*]

1. Department of Electrical Engineering, Suresh Gyan Vihar University, Jaipur 302017, India; agijaipuratul@gmail.com (A.K.); mkgupta72@gmail.com (M.K.G.)
2. Power System Planning Division, Rajasthan Rajya Vidhyut Prasaran Nigam Ltd., Jaipur 302005, India
3. Department of Computer Science and Engineering, Oakland University, Rochester, MI 48084, USA; neerajgupta@oakland.edu (N.G.); npatel@oakland.edu (N.P.)
4. Department of Electrical & Electronics Engineering, University of the Ryukyus, Senbaru, Okinawa 903-0213, Japan; mdanish@lab.u-ryukyu.ac.jp
5. Media Integrated Communication Laboratory, Graduate School of Engineering, Osaka University, Osaka 565-0871, Japan

* Correspondence: opmahela@gmail.com (O.P.M.); b985542@tec.u-ryukyu.ac.jp (T.S.); mahdi.khosravy@nanase.comm.eng.osaka-u.ac.jp (M.K.)

Received: 24 May 2020; Accepted: 3 July 2020; Published: 8 July 2020

check for updates

Abstract: Penetration level of solar photovoltaic (PV) energy in the utility network is steadily increasing. This changes the fault level and causes protection problems. Furthermore, multi-tapped structure of distribution network deployed to integrate solar PV energy to the grid and supplying loads at the same time also raised the protection challenges. Hence, this manuscript is aimed at introducing an algorithm to identify and classify the faults incident on the network of utilities where penetration level of the solar PV energy is high. This fault recognition algorithm is implemented in four steps: (1) calculation of Stockwell transform-based fault index (STFI) (2) calculation of Wigner distribution function-based fault index (WDFI) (3) calculation of combined fault index (CFI) by multiplying STFI and WDFI (4) calculation of index for ground fault (IGF) used to recognize the involvement of ground in a fault event. The STFI has the merits that its performance is least affected by the noise associated with the current signals and it is effective in identification of the waveform distortions. The WDFI employs energy density of the current signals for estimation of the faults and takes care of the current magnitude. Hence, CFI has the merit that it considers the current magnitude as well as waveform distortion for recognition of the faults. The classification of faults is achieved using the number of faulty phases. An index for ground fault (IGF) based on currents of zero sequence is proposed to classify the two phase faults with and without the ground engagement. Investigated faults include phase to ground, two phases fault without involving ground, two phases fault involving ground and three phase fault. Fault recognition algorithm is tested for fault recognition with the presence of noise, various angles of fault incidence, different impedances involved during faulty event, hybrid lines consisting of overhead line (OHL) and underground cable (UGC) sections, and location of faults on all nodes of the test grid. Fault recognition algorithm is also tested to discriminate the transients due to switching operations of feeders, loads and capacitor banks from the faulty transients. Performance of the fault recognition algorithm is compared with the algorithms based on discrete wavelet transform (DWT), Stockwell transform (ST) and hybrid combination of alienation coefficient and Wigner distribution function (WDF). Effectiveness of the fault recognition algorithm is established using a detailed study on the IEEE-13 nodes test feeder modified to incorporate solar PV plant of capacity 1 MW in MATLAB/Simulink. Algorithm is also validated on practical utility grid of Rajasthan State of India.

Keywords: fault recognition; solar photovoltaic energy; power system fault; Stockwell transform; Wigner distribution function

1. Introduction

Penetration level of renewable energy (RE) in the power network of utilities is continuously increasing and expected to be 20% by 2022 [1,2]. Solar photovoltaic (PV) energy is emerging as a best solution to achieve this penetration level in the regions where solar radiation of sufficient intensity is available. However, due to its intermittent characteristics of power generation, it is required to be operated in association with the flywheel, battery, super-capacitors and PV integrated in parallel with the conventional generators [3]. Furthermore, multi-tapped transmission and distribution lines are deployed for grid integration of the solar PV plants and supplying loads at the same time [4]. These have created challenges related to the system protection, reliability and power quality (PQ) [5,6]. The protection challenges are pronounced due to change in nature of the feeders from the passive and radial power flow nature to the active and bidirectional power flow nature (due to integration of solar PV plants near load centers). Hence, with high penetration level of solar energy in the grid, the protection issues are becoming complex. Hence, intelligent fault recognition algorithms are required to be designed to identify and classify the faults incident on the network of utilities where penetration level of solar PV energy is high. In recent years, the signal processing, mathematical and artificial intelligence (AI) methods have been employed for recognition of the faults to design protection schemes for the network of power interfaced with solar PV energy. A detailed study of the schemes used for protection of the grid integrated solar PV plants is reported in [7]. A detailed comparative study of the mother wavelets of DWT to classify the power system faults and to investigate the impacts of type of mother wavelet on accuracy of the algorithm to classify the faults is reported in [8]. An algorithm using current features computed using WDF and alienation coefficient is implemented to protect the transmission line (TL) [9], utility grid in the presence of solar energy [10] and renewable energy (RE) sources-based hybrid grid [11]. This protection scheme has the advantage of low fault recognition time. Harrou et al. [12], introduced a design of protection scheme for direct current (DC) side of the solar PV plant. This is effective to provide protection in the noisy environment. A fault recognition method for both the grid connected and off-grid photovoltaic systems is reported in [13]. This approach is effective for identification of the type and location of the faults with low computational burden. In [14], authors introduced a convolution neural network (CNN)-based protection scheme using current and voltage signals. This is effective for identification of the faults in islanded mode of the micro-grid with solar energy.

In view of above discussed literature review, algorithms implemented for recognition of faults in the presence of solar PV energy has some demerits. It is pointed out from the above discussed literature that most of the fault recognition techniques are based on the use of a single signal processing approaches. Hence, the reported fault recognition methods have one or more demerits which can be overcome by hybridization of the various techniques to combine the merits of the reported method to design a new technique. A DWT supported fault recognition algorithm is reported in [15] which suffers from the problem of generating false tripping signals and reduced performance in the presence of noise. This drawback is mitigated by the use of ST supported algorithm [16]. However, fault detection time of this approach is high and greater compared to time of half cycle. This has been overcome by the hybrid combination of WDF and alienation coefficient [10]. However, the alienation coefficient used in this algorithm has high magnitude for both the healthy and faulty phases at the time of fault incidence. Thereof, a protection algorithm for recognition of faults in the presence of solar PV energy is required which has merits including fast protection, independent of noise, high accuracy and free from false tripping. These have been considered in this research work with main contributions as follows:

- This manuscript is aimed to introduce a protection algorithm to identify and classify the faults incident on the network of utilities where penetration level of the solar PV energy is high.
- This algorithm combines the merits of Stockwell transform and WDF to recognize faults incident in the presence of the solar PV energy using the proposed CFI. Using the number of faulty phases and IGF based on zero-sequence currents, the types of faults are classified effectively.
- Algorithm is so robust that its performance is least affected by the noise and effective to recognize faults with various angles of fault incidence, different impedances involved during faulty event, hybrid lines with OHL and UGC sections, and location of faults on all nodes of the test grid.
- This protection algorithm will not generate tripping commands when the transients due to switching operations of feeders, loads and capacitor banks are present.

Eight sections are used for arranging the contents in this manuscript. Section 1 describes the introduction and contribution of research work. Fault recognition algorithm, STFI, WDFI, CFI and IGF are described in Section 2. IEEE-13 node modified test feeder and solar PV plant are described in Section 3. Simulation results related to implementation of the fault recognition algorithm are discussed in the Section 4. Implementation of fault recognition algorithm to recognize faults in different cases is discussed in Section 5 whereas Section 6 discusses discrimination of switching and faulty transients. Validation of protection algorithm for practical power utility network with penetration of solar energy is discussed in Section 7. It also includes the performance comparison of the proposed protection algorithm with the existing methods. Finally research work is concluded in Section 8.

2. Proposed Fault Recognition Algorithm

The proposed fault recognition algorithm introduced in this manuscript is implemented for detection and classification of faults for the grids with solar PV energy penetration. Fault detection stage can be implemented in three steps which include (1) calculation of Stockwell transform-based fault index (STFI) (2) calculation of Wigner distribution function-based fault index (WDFI), and (3) calculation of proposed combined fault index (CFI) using STFI and WDFI. The STFI and WDFI are the intermediate indices, the advantages of which are combined in the proposed CFI. Main contribution of this paper is CFI, hence the fault recognition results are discussed in detail using the CFI. This CFI is used to detect the faulty events and to identify the faulty phases. Fault classification stage is implemented using the number of faulty phases to classify the different types of faults. Involvement of ground in the two phase faults will be identified using the index for ground fault (IGF). All the steps involved in the proposed protection algorithm are illustrated in the Figure 1.

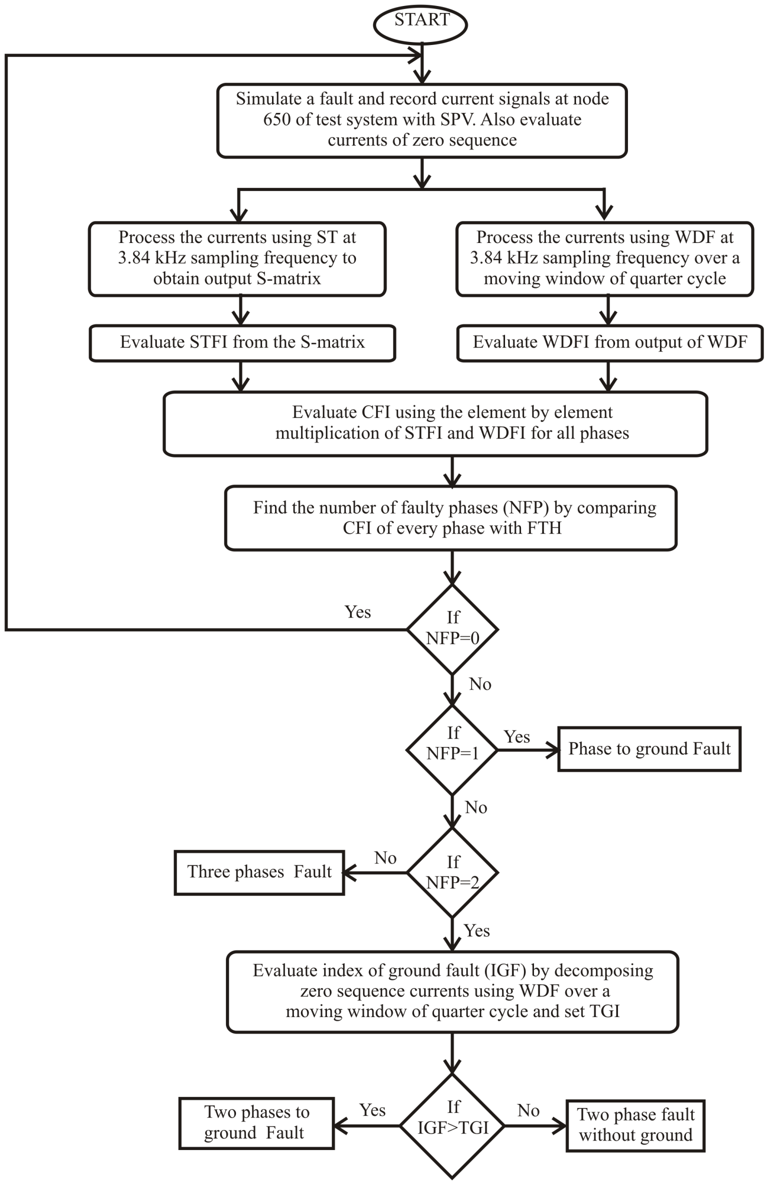

Figure 1. Fault recognition algorithm.

Detailed description of the STFI, WDFI, CFI and IGF is provided in the following subsections.

2.1. Stockwell Transform-Based Fault Index

The current signals measured at node 650, which is considered to be the network protection relay location (NPRL-1), are processed using Stockwell transform for identification of the faulty conditions with the help of Stockwell Transform-Based Fault Index (STFI). The Stockwell Transform (ST) is an extended version of the continuous Wavelet transform (CWT). The ST can also be evaluated with the help of the short time Fourier transform (STFT) [17]. High time resolution at a high frequency and a low time resolution at a low frequency can be obtained using ST [18]. This also has the merit that its performance is least affected by the noise associated with the current signals and effective in identification of the waveform distortions. The STFT of a time variant signal $i(t)$ can be obtained using the below mentioned relation [18].

$$STFT(\tau, f) = \int_{-\infty}^{+\infty} i(t)g(\tau - t)e^{-j2\pi ft}dt \tag{1}$$

where τ and f denote the time of spectral localization and Fourier frequency respectively, and $g(t)$ denotes a window function. The ST can be derived from the above equation by replacing the window function $g(t)$ with the Gaussian function as shown below [19].

$$g(t) = \frac{|f|}{\sqrt{2\pi}} e^{-\frac{f^2 t^2}{2}} \tag{2}$$

Therefore, the ST can be defined as below [20].

$$S(\tau, f) = \int_{-\infty}^{+\infty} i(t) \frac{|f|}{\sqrt{2\pi}} e^{-\frac{f^2(\tau-t)^2}{2}} e^{-j2\pi f t} dt \tag{3}$$

The output of the ST is a matrix with elements of complex nature and designated as *S-matrix*. Information pertaining to frequency and amplitude of the current signals can be derived from this matrix. The STFI is computed from this *S-matrix*. First, the absolute values *S-matrix* (SM) is obtained by taking absolute values of this *S-matrix*.

$$SM = abs(S\text{-}matrix) \tag{4}$$

Median of the matrix SM (STMI) is evaluated as detailed below.

$$STMI = median(SM) \tag{5}$$

The STMI is a row matrix. The summation of 16 samples (for time duration of quarter cycle) is computed, then window is moved by one sample and again summation is computed. This process is repeated till all the samples are used. The row matrix so obtained is designated as STFI. The peak of STFI will appear at center of the window of 16 samples which is at 0.1 s on x-axis of the plot of STFI. Following procedure is used to compute the STFI (Algorithm 1).

Algorithm 1 STFI calculation using moving window

```
for i = 1:k−15 do
    SA = STMI(i:i + 15,1)
    SB = sum(abs(SA));
    SC(i) = max(SB)
end for
```

STFI = SC

The STFI is effective to extract information of the faulty transients and the noisy condition does not affect performance.

2.2. Wigner Distribution Fault Index

The Wigner distribution function-based fault index (WDFI) is evaluated using the Wigner distribution function (WDF) for processing the current signals at sampling frequency (SF) of 3.84 kHz in domain of time-frequency to identify the faulty events. The algorithm is tested for sampling frequencies of 0.96 kHz, 1.92 kHz, 3.84 kHz, and 7.68 kHz. It is observed that for sampling frequencies of 0.92 kHz and 1.92 kHz, performance of the algorithm is reduced, and some results of case studies are not obtained accurately. This is occurred due to loss of the information using fewer samples. It is also observed that for SF of 7.68 kHz, the performance of algorithm is good but the time of calculation is increased due to the large number of samples. This may reduce the speed of protection scheme. Hence, the optimal SF for the algorithm is 3.84 kHz. Wigner distribution function is effective for analysis of the faulty transients. The Wigner distribution function of the current signal $i(t)$ can be given by the following relation [21].

$$W = \int_{-\infty}^{\infty} i(t + \frac{\tau}{2}) i^*(t + \frac{\tau}{2}) e^{-j\omega\tau} d\tau \tag{6}$$

Here, t is used to represent the time (sliding variable), ω is used to represent angular frequency of signal and τ is used to represent the time domain-based signal function. WDF has used a window of 16 samples (quarter cycle period) and moving by one sample for evaluating the WDFI. Peak appears at centers of the window of 16 samples which appears at 0.1 s on the x-axis of WDFI plot. The W is a complex matrix and used to evaluate proposed WDFI using the following relation (Algorithm 2).

Algorithm 2 WDFI calculation using moving window

```
for i = 1:k−15 do
    WA = W(i:i + 15,1))
    WB = sum(abs(WA))
    WC(i) = max(WB)
end for
WDFI = WC
```

The WDFI uses energy density of the current signals to estimate the faults [22]. Hence, it takes care of the current magnitude which is high during the faulty period.

2.3. Combined Fault Index

Combined fault index (CFI) is used to identify the faults present on the power network in the presence of solar PV energy. This is evaluated by multiplication of the WDFI with the STFI, element by element, as detailed below:

$$CFI = WF \times STFI \times WDFI \tag{7}$$

where WF is the weight factor. This WF depends on complexity of the network and penetration level of the solar energy. Hence, it may be selected at the time of installation of protection scheme for a particular network. In this study, for the proposed test system of IEEE-13 nodes interfaced with 1 MW solar PV plant, the WF is considered equal to 4.2×10^5.

A fault threshold magnitude (FTH) equal to 1×10^{16} which is selected by testing the protection algorithm on 40 sets of data for every fault type which is obtained by varying the parameters like angle of fault incidence, impedance during faulty event, location of faults, presence of noise etc. The peak magnitude of CFI for a phase higher compared to the FTH gives information that phase is faulty whereas the peak magnitude of CFI for a phase, lower compared to the FTH gives information that phase is healthy in nature. Hence, CFI plays key role for identification of a fault and to find out the number of faulty phases. A threshold value of 50 for STFI will identify the healthy and faulty phases. Furthermore, a threshold value of 1×10^9 for WDFI will help to identify the healthy and faulty phases. Furthermore, the WDFI and STFI will not always be effective to recognize faulty events with various angles of fault incidence, different impedances involved during faulty event, hybrid lines with OHL and UGC sections and location of faults on all nodes of the test grid. However, the CFI is effective to recognize faulty events during all the scenario of these events. Hence, the CFI has been discussed in the result section in detail and only brief ideas of STFI and WDFI discussed.

Presently, the solar PV energy is integrated to the utility grid in the form of Solar parks which inject high quantum of RE into the power utility network. Furthermore, in the distribution network the solar energy is integrated up to 80% of rated capacity of the distribution feeders. Hence, during the scenario of high Solar energy penetration, the protections issues are observed which can be solved using the proposed method. Integration of the solar energy to the network changes the fault levels and nature of feeders from the passive and radial power flow nature to the active and bidirectional power flow nature (due to integration of the solar PV plants near load centers). This may lead to mis-operation of the conventional relays which can be eliminated using signal processing-based intelligent protection algorithms. The proposed CFI is effective to recognize faulty events in the utility network during the scenario of high penetration of solar energy.

The CFI has the merits of WDFI to take care of current magnitude indicating the severity of faults and merits of STFI to take care of distortion in the waveform from sinusoidal nature to make the protection scheme independent of system parameters. Furthermore, use of the STFI has also reduced the effect of noise in the performance of protection scheme. However, individual use of the WDFI and the STFI may generate false tripping signal in certain operational conditions.

2.4. Index for Ground Fault

The index for ground fault (IGF) is used to discriminate the involvement of ground in the two phase fault conditions. It is calculated in the similar way as the WDFI. However, here the zero-sequence current is used in place of the phase current. The zero-sequence current (I_0) is evaluated from the currents of all the three phases as detailed below.

$$I_0 = \frac{I_1 + I_2 + I_3}{3} \tag{8}$$

where I_1: current associated with phase A, I_2: current associated with phase B, I_3: current associated with phase C. This zero-sequence current is processed using WDF using 3.84 kHz sampling frequency as detailed below.

$$W_0 = \int_{-\infty}^{\infty} I_0(t + \frac{\tau}{2}) I_0^*(t + \frac{\tau}{2}) e^{-j\omega\tau} d\tau \tag{9}$$

Here, t is used to represent the time (sliding variable), ω is used to represent angular frequency of signal and τ is used to represent the time domain-based signal function. The W_0 is a complex matrix and used to evaluate proposed index for ground fault (IGF) using the following relation.

$$IGF = sum(abs(W_0)) \tag{10}$$

A threshold value for IGF (TGI) equal to 2×10^7 is selected for recognizing the involvement of ground in the two phase faults. This TGI is considered after testing the algorithm on 20 sets of data for each of the phase to phase and double phases to ground faults. The IGF corresponding to two phase fault will have the peak magnitude greater than TGI when the ground is involved in the fault.

3. Proposed Test System

Test system of IEEE-13 node distribution network is modified by interfacing a solar photovoltaic (PV) plant on node 680. This is used to perform the proposed study aimed to design a protection scheme which is effective in the presence of solar energy. The test distribution network is rated for a capacity of 5 MVA, 60 Hz frequency and 0.48 kV & 4.16 kV voltage levels. Loads which are balanced and unbalanced in nature are connected to this system [23,24]. Modified distribution feeder is described in Figure 2. The solar PV plant is rated at a capacity of 1 MW and interfaced to the node 680 of the test system through a solar interconnecting transformer (SICT) and an overhead line (OHL) of length 5 km. Parameters of this line used in this study are reported in [11]. There is a distribution interconnecting transformer (DICT) connected between the nodes 633 and 634 where these nodes are maintained at 0.48 kV & 4.16 kV voltages, respectively. This test network is integrated to the utility grid, on node 650, employing a transformer characterized as grid interconnecting transformer (GICT). The utility grid is operated at 115 kV voltage and node 650 is operated at 4.16 kV. The details of these interconnecting transformers (ICTs) is tabulated in Table 1. The high voltage windings of these ICTs are considered to be primary winding (PW) and low voltage windings are considered to be secondary winding (SW). The network protection relay (NPRL-1) is installed on the node 650. Currents are measured on this location and processed continuously using proposed fault recognition algorithm to generate tripping signal during faulty conditions, for operating the circuit breaker (CB) to isolate the faulty section. The network protection relay (NPRL-2) is installed on the node 680 to investigate performance of the fault recognition algorithm at the point of solar PV energy injection.

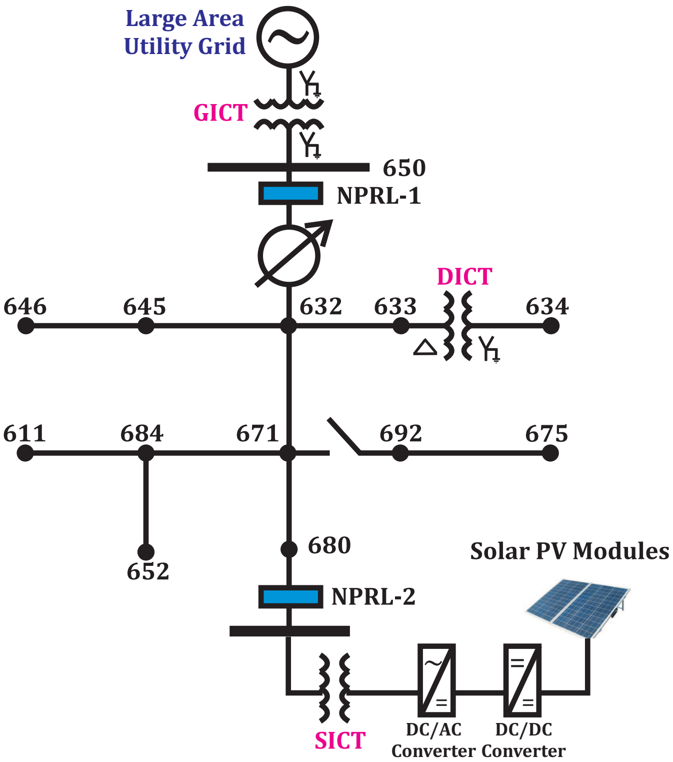

Figure 2. Utility grid interfaced with solar PV plant.

Table 1. Interconnecting Transformers of Test System.

Transformer	MVA	kV	kV	Primary Winding		Secondary Winding	
		PW	SW	R(Ω)	X(Ω)	R(Ω)	X(Ω)
GICT	10	115.00	4.16	29.090	211.65	0.1145	0.8308
DICT	5	4.16	0.48	0.3807	2.7689	0.0511	0.0042
SICT	1	4.16	0.260	0.1730	195.80	0.0008	0.7645

The parameters of OHLs, underground cables, loads, lengths of OHLs and UGCs and feeder configurations as reported in [25,26] are implemented to perform the proposed study. The construction and technical parameters of the solar PV plant are detailed in the following subsection.

Solar PV System

A solar photovoltaic (PV) plant rated at a capacity of 1 MW is integrated to the test system on node 680. The block scheme showing all the stages involved in conversion of the solar energy into electrical energy and injection into the grid is illustrated in Figure 3.

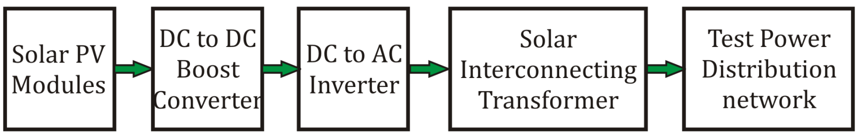

Figure 3. Block scheme of Solar PV energy plant.

The solar modules are used to convert solar energy into the electrical energy in the form of direct current. These modules are consisting of series and parallel combinations of solar cells which are the p-n junctions fabricated in the form of thin layer of semiconductor devices. The characteristics which are followed for their operation are same as the p-n junction and depend on temperature of

PV modules and intensity of solar radiations. Equivalent circuit for the solar cell using the topology composed of a single diode is used in this study. This model approximately represents solar cell and can be effectively used for high solar radiations. However, it has following limitations [27,28]:

- Single-diode model is not efficient when solar irradiance level is low.
- Single-diode model exhibits deteriorating effects at low irradiance levels, especially within the vicinity of the open-circuit voltage of the cell.
- The single-diode model assumes that recombination loss in the depletion region is neglected. However, in a practical solar cell, recombination loss takes place substantially and it becomes significant during the conditions of low voltage.
- Single-diode model of solar cell gives low efficiency during the conditions of partial shading.

The solar PV plant of 1 MW capacity is used which consists of 10 modules each with a 100 kW capacity and combined in parallel mode. The output voltage (V) and current (I) of the solar cell are related to each other as per following relation (single-diode model) [29].

$$I = I_{ph} - I_0 \left\{ exp\left[\frac{q(V + IR_s)}{AkT} \right] - 1 \right\} - \left(\frac{V + IR_s}{R_{sh}} \right) \tag{11}$$

here symbols are represented as follows: I_{ph} is used to represent current of solar cell, I_0 represents saturation current, A is a curve fitting factor, R_{sh} is shunt resistance, R_s is series resistance, q is charge on electron and k is the Boltzmann constant.

Parameters used in this study for the solar PV plant are as V_{oc} = 64.2 V, I_{sc} = 5.96 A, V_{mp} = 54.7 V, I_{mp} = 5.58 A, R_s = 0.037998 Ω, R_{sh} = 993.51 Ω, I_0 = 1.1753 e^{-8} A, diode quality factor Q_d = 1.3, and I_{ph} = 5.9602 A [30]. The V_{mp} and I_{mp} respectively represent the voltage and current at maximum power tracking condition.

The DC to DC boost converter is used to increase the solar PV output voltage of 273.5 V to 500 V DC. The control pulses to this converter are provided with the help of maximum power point tracking algorithm (MPPT) of solar PV system (incremental conductance method). The output of this converter is considered to be input to the DC to AC inverter.

The DC to AC inverter is used to convert the 500 V DC power to the 260 V, 3-phase, 60 Hz AC power. This converter is realized using the 3-leg voltage source converter (VSC) using the insulated gate bipolar transistors (IGBT). A coupling capacitor of 12,000 µF is used between the boost converter and inverter.

The ac output power from the inverter is stepped up to the 4.16 kV with the help of solar interconnecting transformer (SICT), the details of which are provided in Table 1. The output power from the SICT is injected into the utility test system at node 680.

4. Application of Fault Recognition Algorithm for Detection and Classification of Faulty Events

The simulation results for detection and classification of the various faulty events incident on the power network with integrated solar power plant are discussed in this section. Incident faults have been simulated on the test node 675 and currents are measured on test node 650 (NPRL-1 location).

4.1. Fault Between Phase A and Ground

Faulty event is simulated between phase A and ground (AG fault) on test node 675 at 0.1 s (6th cycle). Measurement of currents associated with all the phases is performed on test node 650 (NPRL-1 location). These current signals are decomposed using proposed fault recognition algorithm using the Wigner distribution function and proposed WDFI is evaluated. Similarly, these current signals are decomposed using the Stockwell transform and proposed STFI is evaluated. Proposed combined fault index (CFI) is evaluated using element by element multiplication of the WDFI and STFI. The current signals, WDFI, STFI, and CFI during the phase A to ground faulty event are illustrated in Figure 4. A look at Figure 4a indicates that faulty event on phase A increases the current of this phase at

6th cycle whereas the current of phases B and C still has steady state values. This indicates that phase A is faulty in nature whereas the phases B and C are healthy. The WDFI shown in Figure 4b, indicates that values of this index are low for the healthy period. Magnitude of this index increases due to the incidence of phase A to ground faulty event. However, this continues to have low values for the phases B and C even after fault incidence. This is inferred from the Figure 4c that values of STFI are low for the healthy period of network. Magnitude of this index increases corresponding to all phases due to the incidence of phase A to ground fault. However, increase in magnitude of STFI is high for the faulty phase A compared to the healthy phases. Figure 4d details the combined fault index evaluated from the WDFI and STFI. This is concluded that CFI has peak magnitude above the threshold for the faulty phase A and below the threshold for the healthy phases B and C. Hence, proposed fault recognition algorithm making use of the current features extracted with the help of Wigner distribution function and Stockwell transform effectively recognizes the faulty event including phase A and ground. This is also effective in discriminating the faulty and healthy phases.

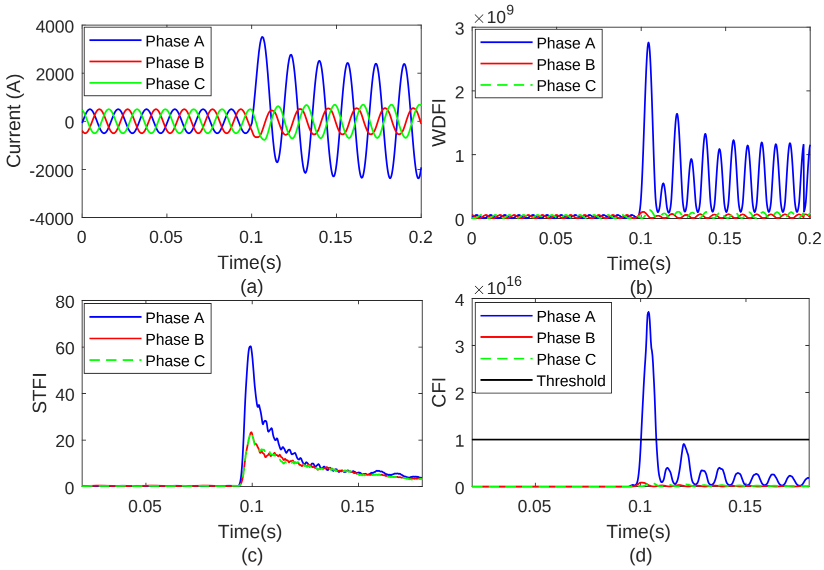

Figure 4. Detection of fault incident between phase A and ground (**a**) current waveform (**b**) WDFI (**c**) STFI (**d**) CFI.

To evaluate the fault detection time, the high-resolution plot of combined fault index is illustrated in Figure 5. It is observed that CFI crosses the threshold magnitude within time duration of a quarter cycle because WDF has used a window of 16 samples (quarter cycle period) and moving by one sample for evaluating the WDFI. Hence, fault will be identified within time duration of 0.00417 s (quarter cycle). Therefore, proposed fault recognition algorithm is effective in identification of the AG fault within a time period of quarter cycle.

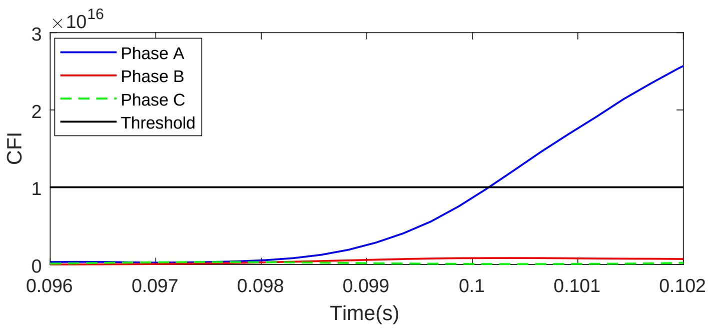

Figure 5. Estimation of time involved during phase A to ground faulty event.

4.2. Fault Between Phase A and Phase B

Faulty event is simulated between phase A and phase B (AB fault) on test node 675 at 0.1 s (6th cycle). Measurement of currents associated with all the phases is performed on test node 650 (NPRL-1 location). These current signals are decomposed using proposed fault recognition algorithm using the Wigner distribution function to compute WDFI. The current signals are decomposed using the Stockwell transform to compute STFI. Proposed combined fault index (CFI) is evaluated using element by element multiplication of the WDFI and STFI. The current signals, WDFI, STFI, and CFI during the phase A to phase B faulty event are described in Figure 6. This is observed from Figure 6a that faulty event on phase A and phase B increases the current of these phases at 6th cycle whereas the current of phase C still has steady state values. This indicates that phases A and B are faulty whereas the phase C is healthy. The WDFI shown in Figure 6b, indicates that values of this index are low corresponding to all phases during the healthy period of network. This index magnitude increases for A and B phases due to phase A to phase B faulty event. However, this continues to have low values for the phase C even after fault incidence. This can be concluded from the Figure 6c that magnitudes of STFI are low for the healthy period of network. Magnitude of this index increases corresponding to phases A and B due to the incidence of phase A to phase B fault. However, increase in magnitude of STFI is low for the healthy phase C compared to the faulty phases. Figure 6d details the combined fault index evaluated from the WDFI and STFI. This is concluded that CFI has peak magnitude above the threshold for the faulty phases A and B. The CFI has values below the threshold for the healthy phase C. Hence, proposed fault recognition algorithm effectively recognizes the faulty event including phase A and phase B. It also effectively discriminates the faulty and healthy phases. Furthermore, the event of phase A to phase B fault has been detected in a time period of quarter cycle.

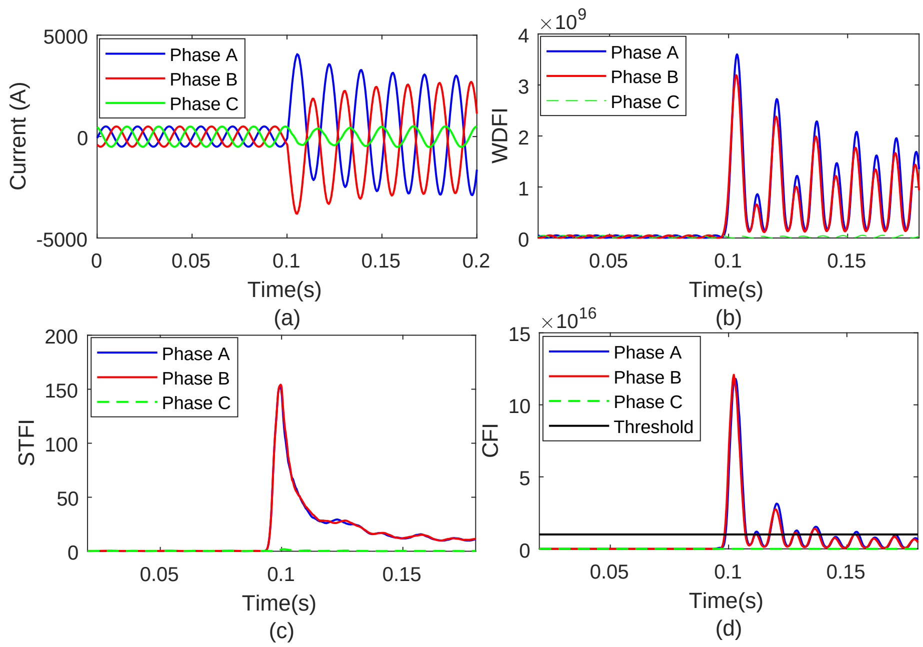

Figure 6. Detection of fault incident between phase A and phase B (**a**) current waveform (**b**) WDFI (**c**) STFI (**d**) CFI.

4.3. Fault Between Phases A and B to Ground

Faulty event is simulated between phases A and B to ground (ABG fault) on test node 675 at 0.1 s (6th cycle). Measurement of currents associated with all the phases is performed on test node 650 (NPRL-1 location). These current signals are decomposed using proposed fault recognition algorithm using the Wigner distribution function to compute WDFI. These current signals are decomposed using the Stockwell transform to compute STFI. The combined fault index (CFI) is evaluated using element by element multiplication of the WDFI and STFI. The current signals, WDFI, STFI and CFI during the event of ABG fault are described in Figure 7. This is observed from Figure 7a that faulty event on phases A and B to ground increases the current of these phases at 6th cycle whereas current of the phase C still has steady state value. This indicates that phases A and B are faulty whereas the phase C is healthy. The WDFI shown in Figure 7b, indicates that values of this index are low corresponding to all the phases during period of healthy condition of the network. Magnitude of this index increases for the phases A and B due to the incidence of ABG faulty event. However, this index continues to have low values for the phase C even after ABG fault incidence. This can be concluded from the Figure 7c that magnitudes of STFI for all phases are low for the healthy period of network. Amplitude of this index increases for phases A and B due to the incidence of ABG fault. However, increase in magnitude of STFI is low for the healthy phase C compared to the faulty phases. Figure 7d details the combined fault index evaluated from the WDFI and STFI. This is concluded that CFI has peak magnitude above the threshold for the faulty phases A and B. The CFI has peak value below the threshold for the healthy phase C. Hence, proposed fault recognition algorithm effectively recognizes the ABG faulty event and discriminates the faulty and healthy phases. Furthermore, the event of ABG fault has been detected in a time period of quarter cycle.

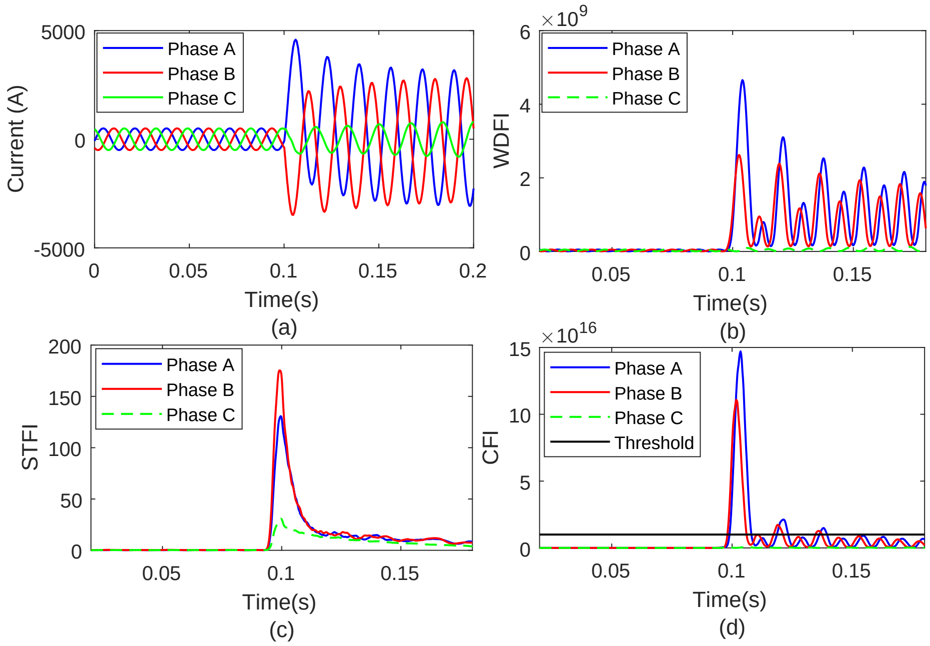

Figure 7. Detection of fault incident between phases A and B to ground (**a**) current waveform (**b**) WDFI (**c**) STFI (**d**) CFI.

4.4. Fault Involving all the Phases and Ground

Faulty event involving all the phases and ground (ABCG) is simulated on the test node 675 at 0.1 s (6th cycle). Measurement of currents associated with all the phases is performed on test node 650 (NPRL-1 location). These current signals are decomposed using proposed fault recognition algorithm using the Wigner distribution function and proposed WDFI is evaluated. Similarly, these current signals are decomposed using the Stockwell transform to evaluate the proposed STFI. Proposed combined fault index (CFI) is evaluated using element by element multiplication of the WDFI and STFI. The current signals, WDFI, STFI and CFI during the event of ABCG fault are described in Figure 8. This is observed from Figure 8a that ABCG faulty event increases the current of all the phases at 6th cycle. This indicates that all the phases are faulty. The WDFI shown in Figure 8b, indicates that values of this index are low corresponding to all the phases during period of healthy condition of network. This index magnitude increases for all the phases due to the incidence of ABCG faulty event.

This can be concluded from the Figure 8c that magnitudes of STFI for all the phases are low for the healthy period of network. This index magnitude increases corresponding to all phases due to the incidence of ABCG fault. Figure 8d details the combined fault index evaluated from the WDFI and STFI. This is concluded that CFI has peak magnitude above the threshold for all the phases indicating that every phase has a faulty nature. Hence, proposed fault recognition algorithm effectively recognizes the ABCG faulty event. Furthermore, the event of ABCG fault has been detected in a time period of quarter cycle.

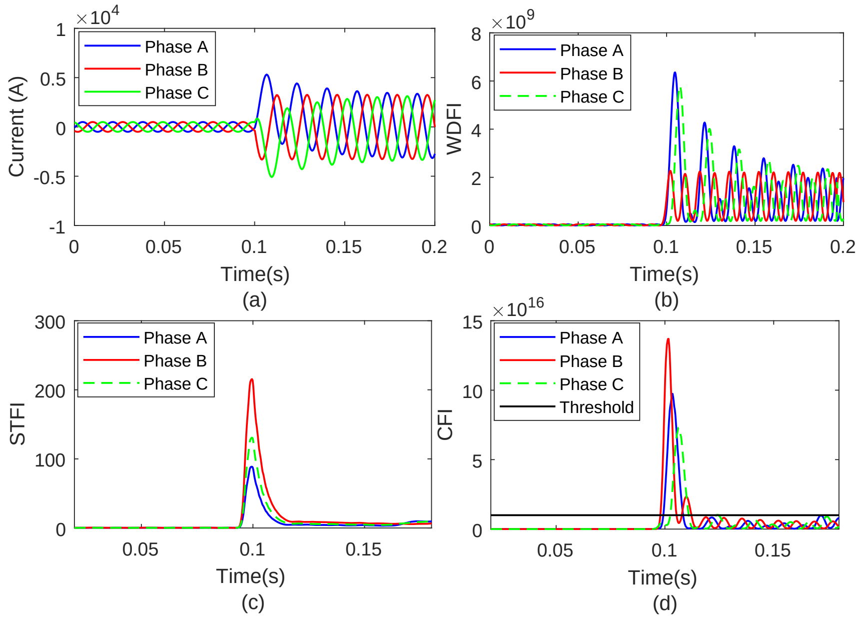

Figure 8. Detection of fault involving all the phases and ground (**a**) current waveform (**b**) WDFI (**c**) STFI (**d**) CFI.

4.5. Classification of Faulty Events

Types of faulty events have been recognized by identifying the number of faulty phases. If all the three phases have the peak magnitude of CFI greater than the fault threshold (FTH) then ABCG fault is present. During the faulty event when CFI has peak magnitude greater than FTH corresponding to one phase only then one phase to ground fault (AG, BG or CG) is present. Phase involved in the faulty event will have the peak CFI greater than FTH. Hence, faulty phase can be identified easily. There exist two faulty phases during AB or BC or CA fault event and two phases to ground (ABG or BCG or CAG) fault. These faults can be discriminated from each other using the IGF as described in Figure 9. This is concluded that the IGF corresponding to two phase fault involving ground will have the peak magnitude greater than the threshold value of IGF which is selected as 2×10^7 for this study. However, all the two phase faults which are not involving the ground will have peak magnitude lower than the TGI. Hence, proposed approach succeeded to identify and classify all the types of faulty events on the power system in the presence of solar power generation.

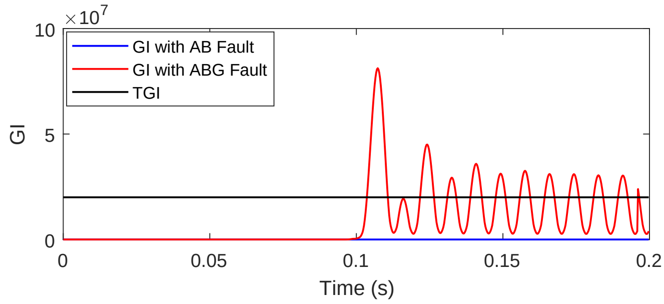

Figure 9. Index for ground fault classifying AB and ABG faults.

5. Case Studies: Implementation of Fault Recognition Algorithm

Performance of the fault recognition algorithm is analyzed for different cases of fault incidence. These include availability of wide range of fault impedance, fault incidence at different angles with respect to the sinusoidal waveform of current, fault incident at all nodes of the test network, fault incident in noisy environment and fault incident at node where solar energy is injected. Faults have also been investigated when travelling waves follow the path through hybrid line which has sections of overhead line (OHL) as well as underground cable (UGC). The AG fault is discussed in this section for all the cases of study and current measurements are performed on test node 650. However, algorithm effectively identified all the fault types.

5.1. Faulty Events with Different Fault Impedance

The impedance involved during the incidence of faulty event affects the performance of fault recognition algorithm. Therefore, it becomes essential to test the algorithm for different possible values of fault impedance. Hence, performance of the fault recognition algorithm is evaluated by considering 0 Ω, 1 Ω, 2 Ω, 4 Ω, 5 Ω and 10 Ω fault impedances for all types of faults. However, results are discussed for AG fault incident on node 675 and CFI for all values of fault impedance is included in Table 2. It is observed that CFI associated with the phase A has values high compared to the pre-set threshold magnitude of 1×10^{16}. However, peak magnitude of CFI associated with the healthy phase B and phase C is low compared to pre-set threshold. Hence, AG fault has been identified effectively in the availability of high fault impedance up to 10 Ω.

Table 2. Performance of Fault Recognition Algorithm with Variable Fault Impedance.

Phase Name	**Peak Magnitude of CFI (AG Fault)**					
	0 Ω	**1 Ω**	**2 Ω**	**4 Ω**	**5 Ω**	**10 Ω**
Phase A	3.728×10^{16}	3.552×10^{16}	3.378×10^{16}	2.988×10^{16}	2.819×10^{16}	2.005×10^{16}
Phase B	8.314×10^{13}	6.995×10^{13}	5.847×10^{13}	4.0318×10^{13}	3.925×10^{13}	9.107×10^{12}
Phase C	7.302×10^{13}	6.226×10^{13}	5.339×10^{13}	3.564×10^{13}	1.107×10^{13}	7.003×10^{12}

5.2. Faulty Event at Different Locations of Test Network

Performance of the algorithm is tested for location of faults on all nodes of the test system. Results of the AG fault are discussed in this section. However, algorithm is also effective in identification of AB, ABG, and ABCG faults simulated on all nodes of the test system. CFI is discussed for nodes 634 and 652 as hazardous faulty locations. Line between the nodes 652 and 650 is a hybrid line which comprises of the overhead (OH) line and underground (UG) cable. CFI evaluated at node 650 when the fault is incident on the node 652 is illustrated in Figure 10. This is observed that CFI has peak magnitude above the threshold for the faulty phase A and below the threshold for the healthy phases B and C. Hence, proposed fault recognition algorithm making use of the current features extracted with the help of Wigner distribution function and Stockwell transform effectively recognizes the faulty event including phase A and ground with OH-UG hybrid line between the faulty node and protection relay location.

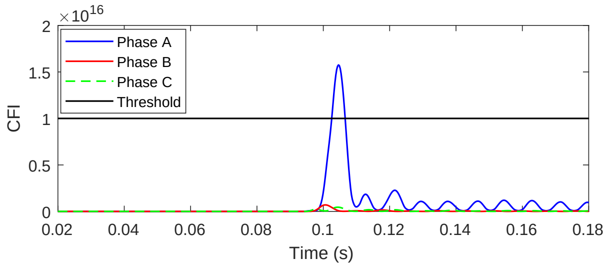

Figure 10. Combined fault index with AG fault on node 652 of test system.

The CFI with AG fault on node 634 is also discussed because there is a transformer between the faulty node 634 and node 650 where currents are recorded. CFI evaluated at node 650 when the fault is incident on the 634 is described in Figure 11. This is observed that CFI has peak magnitude above the threshold for the faulty phase A and below the threshold for the healthy phases B and C. Hence, proposed fault recognition algorithm making use of the current features extracted with the help of Wigner distribution function and Stockwell transform effectively recognizes the faulty event including phase A and ground in the presence of a transformer between the nodes with fault and protection relay.

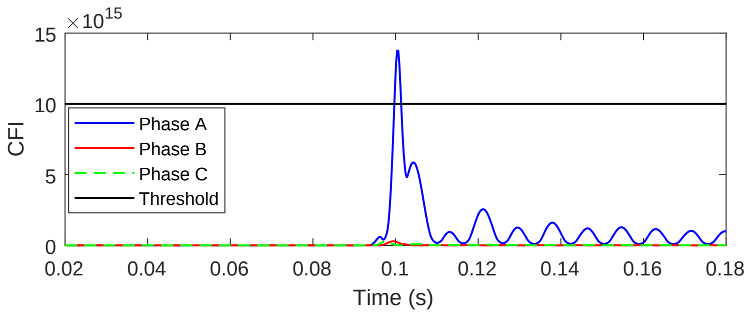

Figure 11. Combined fault index with AG fault on node 634 of test system.

Application of the algorithm is generalized by recognizing the faults on all nodes of the test network. The AG fault is simulated at all nodes and current recorded on node 650 is processed to evaluate the CFI. The peak magnitude of the CFI for incidence of fault on all the nodes is provided in Table 3. This is observed that CFI associated with the phase A is above the FTH for location of fault on all the nodes. However, the peak magnitude of CFI associated with the phases B and C is observed to be below the FTH. Hence, proposed fault recognition algorithm making use of the current features extracted with the help of Wigner distribution function and Stockwell transform effectively recognizes the faulty events at all nodes of the test system in the presence of solar PV energy.

Table 3. Performance of Fault Recognition Algorithm with AG Fault at Different Nodes of the Test System.

Phase Name	Peak Magnitude of CFI (AG Fault)										
	646	**645**	**633**	**634**	**611**	**684**	**652**	**671**	**680**	**692**	**675**
Phase A	7.005×10^{16}	8.127×10^{16}	8.534×10^{16}	1.377×10^{16}	1.814×10^{16}	3.723×10^{16}	1.568×10^{16}	3.554×10^{16}	2.016×10^{16}	3.546×10^{16}	3.728×10^{16}
Phase B	1.102×10^{14}	1.529×10^{14}	2.027×10^{14}	2.885×10^{13}	1.297×10^{14}	1.301×10^{14}	6.965×10^{14}	1.759×10^{14}	4.445×10^{13}	1.762×10^{14}	8.314×10^{13}
Phase C	1.642×10^{14}	2.291×10^{14}	2.782×10^{14}	2.642×10^{13}	9.733×10^{13}	1.106×10^{14}	4.488×10^{14}	1.317×10^{14}	3.785×10^{13}	1.354×10^{14}	7.302×10^{13}

5.3. Faulty Events with Different Angles of Fault Incidence

Performance of the fault recognition algorithm is evaluated at different angles of fault incidence to generalize the applicability of the method. All fault types are analyzed for incidence angles of 0°, 45°, 90°, and 135°. However, results for AG fault incident at test node 675 are discussed and peak values of CFI are detailed in Table 4. From this table, it is inferred that peak magnitude of CFI associated with phase A is high compared to pre-set threshold (1×10^{16}) for all angles of fault incidence. However, peak magnitude of CFI for the phase B and phase C is low in comparison to the pre-set threshold. Therefore, it is concluded that the AG fault is identified with high accuracy at different angles of fault incidence. Furthermore, healthy and faulty phases are also discriminated from each other for all angles of fault incidence.

Table 4. Performance of Fault Recognition Algorithm with Variable angle of Fault Incidence.

Phase Name	Peak Magnitude of CFI (AG Fault)			
	0°	**45°**	**90°**	**135°**
Phase A	3.728×10^{16}	5.521×10^{16}	4.428×10^{16}	3.165×10^{16}
Phase B	8.314×10^{13}	1.447×10^{14}	5.905×10^{13}	6.673×10^{13}
Phase C	7.302×10^{13}	1.553×10^{14}	1.036×10^{14}	4.279×10^{13}

5.4. Performance of Protection Algorithm in the Noisy Environment

AG fault is simulated on node 675 of test network and currents are recorded on node 650. A noise of 10 dB SNR is added to these current signals. These current signals with superimposed noise of 10 dB SNR are processed using the proposed fault recognition algorithm to examine performance of the algorithm in the presence of noise. These current signals are decomposed using proposed fault recognition algorithm using the Wigner distribution function to compute WDFI. Similarly, these current signals are decomposed using the Stockwell transform and STFI is evaluated. Proposed combined fault index (CFI) is computed using element by element multiplication of the WDFI and STFI. The current signals, WDFI, STFI, and CFI during the phase A to ground faulty event are illustrated in Figure 12. A look at Figure 12a indicates that faulty event on phase A increases the current of this phase at 6th cycle whereas the current of phases B and C still has steady state values. This indicates that phases A is faulty whereas the phases B and C are healthy. The WDFI shown in Figure 12b, indicates that values of this index are low for the healthy period of network. Magnitude of this index increases due to incidence of the phase A to ground faulty event. However, this continues to have low values for the phases B and C even after fault incidence. This is inferred from the Figure 12c that values of STFI are low for the healthy period of network. Magnitude of this index increases corresponding to all phases due to the incidence of phase A to ground fault. However, increase in magnitude of STFI is high for the faulty phase A compared to the healthy phases. Figure 12d details the combined fault index evaluated from the WDFI and STFI. This is concluded that CFI has peak magnitude above the threshold for the faulty phase A and below the threshold for the healthy phases B and C. Hence, proposed protection algorithm to recognize the faulty event including phase A and ground even under the high noise level of 10 dB SNR. Furthermore, the algorithm also successfully identified the AG, AB, ABG, and ABCG faults.

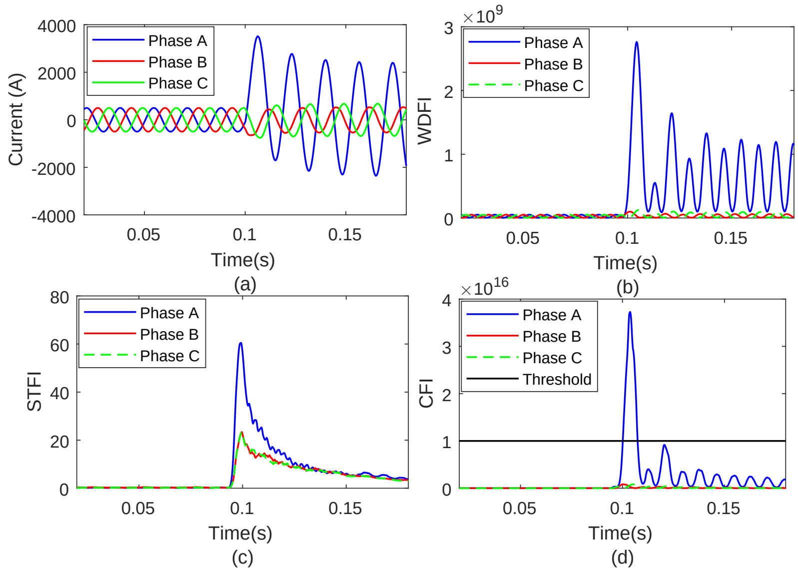

Figure 12. Detection of AG fault on node 675 in noisy environment (**a**) current waveform (**b**) WDFI (**c**) STFI (**d**) CFI.

5.5. Recognition of Faulty Event Using Currents Measured at Node of Solar Energy Injection

AG fault is simulated on node 675 of test network and currents are recorded on node 680 where the solar PV plant is integrated to the test network. These current signals are processed using the proposed fault recognition algorithm to investigate the effectiveness of the algorithm at node of solar energy injection. The combined fault index evaluated is illustrated in Figure 13. This is concluded that CFI has peak magnitude above the threshold for the faulty phase A and below the threshold for the healthy phases B and C. Hence, proposed fault recognition algorithm is found to be effective to recognize the faulty event including phase A and ground using the current measurements on node 680 to which solar PV plant is integrated.

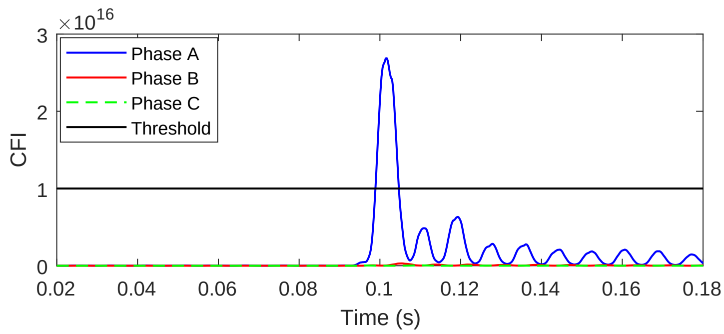

Figure 13. The CFI evaluated by recording currents on node of solar energy injection for detection of AG fault simulated on node 675.

6. Performance of Protection Algorithm in the Presence of Switching Transients

This section presents the detailed results to investigate effectiveness of the algorithm in discriminating transients of switching from the transients associated with the faulty conditions.

6.1. Feeder Operation

Operation of the feeder is realized using the circuit breaker (CB) installed between the node 692 and the node 671. This switch is switched off at 4th cycle to perform feeder tripping and switched on at 6th cycle to perform feeder re-closing. Performance of the algorithm is evaluated for a duration of 12 cycles and respective results are detailed in Figure 14. Figure 14a illustrates that current magnitude decreases after tripping of the feeder due to reduction in load. Furthermore, waveform distortion is observed at the moments of feeder operation. Waveform distortion is pronounced at the moment of feeder re-closing compared to feeder tripping. Figure 14b details that the magnitude of WDFI is decreased for the duration when feeder remains tripped (i.e., from 4th to 6th cycles). However, magnitude of WDFI increases for a short duration at the instants of feeder tripping as well as re-closing. Figure 14c described that STFI has high magnitude at the moments of feeder tripping and re-closing. Figure 14d illustrates that CFI possesses comparatively high magnitudes in the time of feeder tripping and re-closing. However, this CFI peak amplitude is lower compared to the pre-set threshold for identification of the faulty phenomenon. Hence, fault recognition algorithm introduced in this manuscript effectively differentiates the faulty and switching transients. The trip signal will be generated when faulty transients are present and trip signal will not be generated when the switching transients are present.

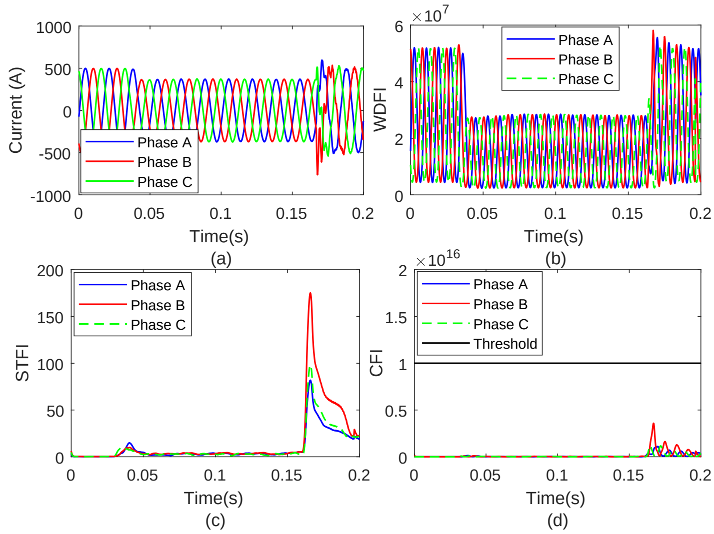

Figure 14. Event of feeder operation (**a**) current waveform (**b**) WDFI (**c**) STFI (**d**) CFI.

6.2. Capacitor Bank Operation

Operation of the capacitor bank is realized by switching off the capacitor of 600 kVAr connected to network on node 675 at 4th cycle and again switching on at 6th one. Performance of the algorithm is evaluated for a duration of 12 cycles and respective results are detailed in Figure 15. Figure 15a illustrates that current magnitude increases after switching off the capacitor due to low power factor which regains normal values at 6th cycle when capacitor is switched on again. Furthermore, the waveform distortion is observed at the moments of capacitor bank operation. Waveform distortion is pronounced at the moment of switching on the capacitor bank compared to switching off the capacitor. Figure 15b details that the magnitude of WDFI is increased for the duration when capacitor remains switched off (i.e., from 4th to 6th cycles). However, magnitude of WDFI increases for a short duration at the instants of capacitor operation. Figure 15c described that STFI has high magnitude at the moments of capacitor bank switching off as well as switching on. Figure 15d shows that the CFI has comparatively high amplitude when capacitor is switched on. However, this CFI peak magnitude is lower compared to the pre-set threshold used for identification of faulty phenomenon. Hence, fault recognition algorithm introduced in this manuscript effectively differentiates the faulty transients and capacitor switching transients. The trip signal will be generated when faulty transients are present and trip signal will not be generated when the capacitor switching transients are present.

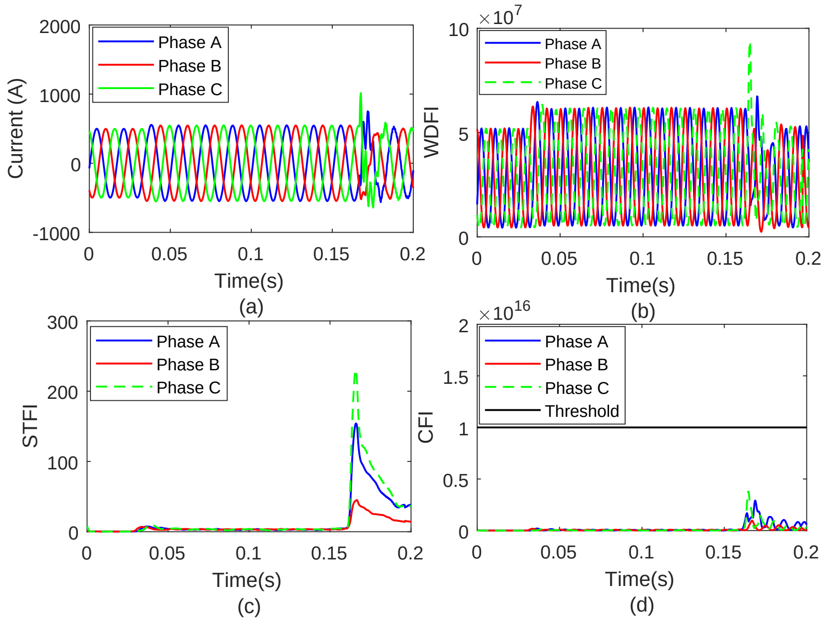

Figure 15. Event of capacitor switching (**a**) current waveform (**b**) WDFI (**c**) STFI (**d**) CFI.

6.3. Operation of Load Switching

The load operation is performed via switching off the 1155 kW + 660 kVAr load that is connected to network on node-671 in 4th cycle and next switching on at 6th cycle. Performance of the algorithm is evaluated for a duration of 12 cycles and respective results are detailed in Figure 16. Figure 16a illustrates that current magnitude decreases after switching off the load due to low power factor which regains normal values at 6th cycle when load is switched on again. Furthermore, waveform distortion is observed at the moments of load operation. Waveform distortion is pronounced at the moment of load switching on compared to switching off the load. Figure 16b details that the magnitude of WDFI is decreased for the duration when load remains switched off (i.e., from 4th to 6th cycles). However, magnitude of WDFI increases for a short duration at the instants of load operation. Figure 16c described that STFI has high magnitude at the moments of load switching off as well as switching on. Figure 16d shows that the CFI has slight high magnitude while load switching. However, this CFI peak magnitude is very low compared to the pre-set threshold used for identification of faulty phenomenon. Hence, fault recognition algorithm introduced in this manuscript effectively differentiates the faulty transients and load switching transients. The trip signal will be generated when faulty transients are present and trip signal will not be generated when the load switching transients are present.

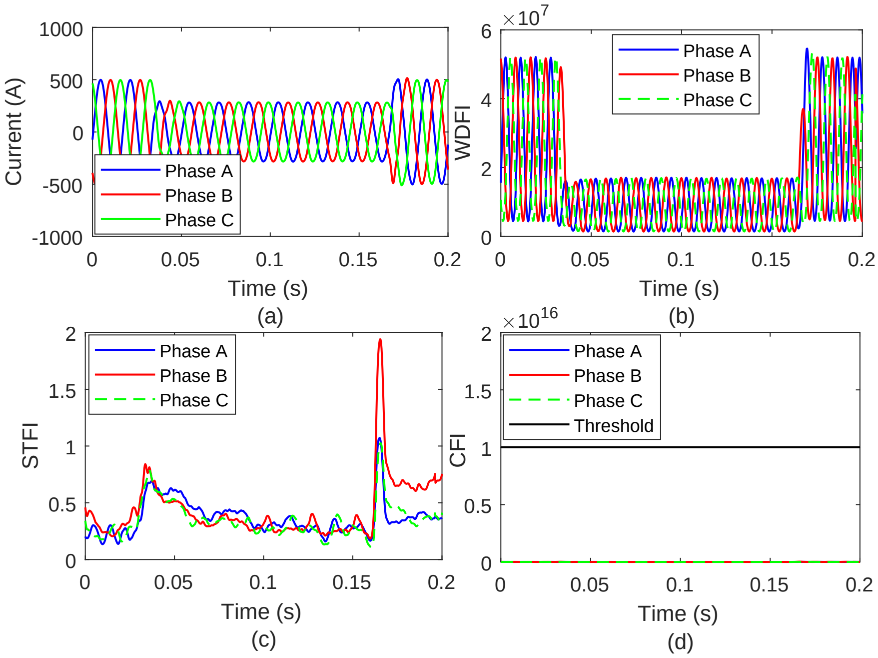

Figure 16. Event of load switching (**a**) current waveform (**b**) WDFI (**c**) STFI (**d**) CFI.

7. Validation of Fault Recognition Protection Algorithm

This section briefly discussed the application of the proposed algorithm to large sized power system. Performance of the algorithm is also compared with the methods reported in the literature to show the effectiveness of the proposed fault Recognition algorithm.

7.1. Application to Practical Large Size Power System

Algorithm is tested on the practical power system network of the Rajasthan state of India. This network consists of 765 kV, 400 kV, 220 kV and 132 kV grid substation (GSS) which are interconnected through the AC transmission lines rated at voltage levels of 765 kV, 400 kV, 220 kV and 132 kV. Conventional and renewable energy generators are integrated to this network. An overview of the practical transmission system of Rajasthan State describing the number of grid substations (GSS) and circuit length of the transmission lines is detailed in Table 5. Capacity of the generators integrated to the Rajasthan State transmission system including thermal power stations (TPS), nuclear power stations (PS), hydro and renewable energy (RE) is included in Table 6 [31]. In western parts of the Rajasthan state (Bhadla region), the solar energy is integrated to this grid network in bulk amount. This network is modelled in MiPower software considering all the elements such as transformers, lines, thermal generators, nuclear generators, renewable energy generators, reactors, loads and capacitors [9,10]. Phase A to ground fault is realized on the 220 kV Kanasar–Bhadla line and current is measured on the Bhadla end of the lines. This current signal is decomposed using the proposed algorithm to compute the proposed CFI which is illustrated in Figure 17. This is inferred that peak magnitude of the CFI associated with the phase A is greater than FTH whereas the peaks of CFI associated with the phases B and C are lower than FTH. Hence, the proposed algorithm has identified the fault on the 220 kV transmission line of a practical test system. Fortunately, the weight factor used for computing the CFI works well for the real time network. However, this factor may be adjusted if required. This algorithm can be applied to real world power system network using the microprocessor-based protection relays.

Table 5. Number of Grid Substations and Circuit Length of Transmission Lines in Rajasthan.

Voltage Level (kV)	Number of Grid Substation	Total Circuit Length of Lines (km)
765 kV	6	425.498
400 kV	27	7604.444
220 kV	124	15,443.394
132 kV	459	18,245.566
Total	616	41,718.902

Table 6. Generation Capacity Integrated to Transmission System of Rajasthan.

Type of Power Station	Capacity (MW)	Total Generation Contribution (%)
Coal TPS	11,918.45	56%
Gas TPS	824.60	4%
Nuclear PS	456.74	4%
Hydro PS	1961.95	9%
Wind Generation	3734.10	18%
Solar Generation	2178.10	10.29%
Biomass Generation	101.95	0.48%
Total	21,175.90	100%

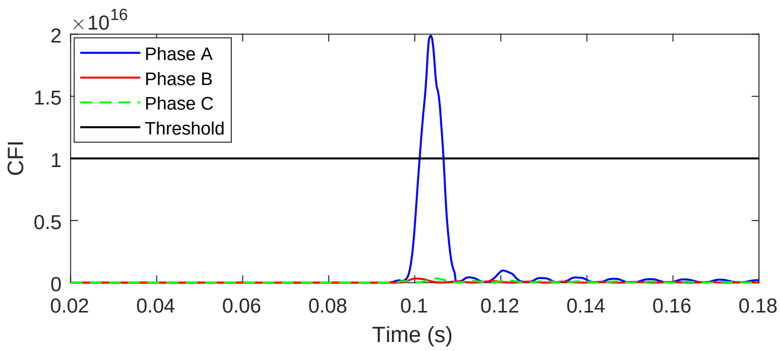

Figure 17. CFI computed during the event of phase A to ground fault on the 220 kV Kanasar–Bhadla line of practical power system network of Rajasthan State of India.

7.2. Performance Comparison

Fault identification and classification capability of the presented fault recognition algorithm is analyzed in comparison to algorithms based on discrete wavelet transform, Stockwell transform and combination of WDF and alienation coefficient reported in [10,15,16] respectively. It is pointed out that the DWT supported algorithm reported in [15] identify the faults using the combination of detailed and approximation coefficients at first decomposition level. Range of the variation of peak is very wide ranging from 1 to 500. Hence, this algorithm sometimes generates false tripping signals. Furthermore, performance of this algorithm is also affected by noisy condition that may generate false tripping signals. This DWT-based fault recognition technique performs well for a noise level lower than 50 dB, SNR. Its performance is adversely affected in the presence of noise higher than 50 dB SNR. This drawback is overcome by the Stockwell transform-based algorithm reported [16]. However, fault detection time of this approach is high and greater than half cycle. This has been overcome by the hybrid combination of WDF and alienation coefficient in [10]. However, the alienation coefficient used in this algorithm has high magnitude for both the healthy and faulty phases at the time of fault incidence. This has been overcome in the fault recognition algorithm introduced in this manuscript. Hence, Stockwell transform and WDF supported fault recognition algorithm introduced in this manuscript overcomes the demerits of algorithms reported in [10,15,16]. Performance comparative study between different fault recognition methods is provided in Table 7. It is observed that performance of proposed method is least affected by noise and it is fast compared to methods reported in [10,15,16].

Table 7. Performance Comparative Study of Fault Recognition Techniques.

Technique	Reference	Performance Parameters	
		Noise Level for Which Performance of the Technique Is Not Affected	**Fault Identification Time (in second)**
DWT	[15]	50 dB SNR	0.0053 s
ST	[16]	20 dB SNR	0.0257 s
WDF + Alienation Coefficient	[10]	10 dB SNR	0.0125 s
ST + WDF	Proposed	10 dB SNR	0.00417 s

8. Conclusions

A hybrid fault recognition algorithm making use of current features extracted using the Stockwell Transform and Wigner distribution function is introduced in this manuscript for recognition of faults on the grid in the presence of solar energy. A combined fault index (CFI) which is obtained from the Stockwell transform fault index (STFI) and Wigner distribution fault index (WDFI) is used to identify the faulty events. This is also used for discriminating faulty phases from the healthy phases. A ground fault index based on currents of zero sequence is introduced to classify the faults of two phases for both involving and not involving the ground. The faults such as phase to ground, two phases fault without involving ground, two phases fault involving ground and three phase fault are successfully identified and classified in the presence of solar energy using CFI. Faults are classified successfully using the number of faulty phases and IGF. This is established that protection algorithm accurately identifies the faults at high speed within a time period of quarter cycle in the presence of solar (SE) generation. Proposed algorithm is effective for fault recognition even in the noisy environment, various angle of fault incidence, different impedances involved during faulty event, hybrid lines with OHL and UGC sections and location of faults on all nodes of the test grid. Fault recognition algorithm efficiently distinguishes the transients resulting from the switching operations of feeders, loads and capacitor banks from the faulty transients. Performance of the fault recognition algorithm is compared with the algorithms reported in the literature and it is established that proposed algorithm has some merits compared to the algorithm based on DWT, Stockwell transform and hybrid combination of alienation coefficient and WDF. Effectiveness of the algorithm is established by a detailed study on the IEEE-13 node test system interfaced with solar PV energy and validated on practical utility grid of the Rajasthan State of India.

Author Contributions: Conceptualization, A.K., O.P.M. and M.K.G.; methodology, A.K., O.P.M. and M.K.G.; software, A.K., O.P.M. and M.K.G.; validation, A.K., O.P.M.; formal analysis, A.K. and O.P.M.; investigation, A.K. and O.P.M.; resources, M.K.G., N.G. and M.K.; data curation, A.K., O.P.M. and N.P.; writing–original draft preparation, A.K., and O.P.M.; writing–review and editing, M.K.G., N.P., N.G., M.K., M.S.S.D., and T.S.; visualization, M.K.G., N.P., N.G., M.K., M.S.S.D., and T.S.; supervision, M.K.G., M.S.S.D. and T.S. All authors have read and agreed to the published version of the manuscript.

Funding: This research received no external funding.

Conflicts of Interest: The authors declare that they have no known conflict of interest.

Abbreviations

Abbreviations used in this article are detailed below:

AC	Alternating current
AG	Phase A and ground
AB	Phase A and phase B
ABG	Phase A and B to ground
ABCG	All the three phases and ground
AI	Artificial intelligence
CB	Circuit breaker
CFI	Combined fault index
CNN	Convolution neural network
CWT	Continuous Wavelet transform
DC	Direct current
DICT	Distribution interconnecting transformer
DWT	Discrete Wavelet transform
FTH	Fault threshold
GICT	Grid interconnecting transformer
GSS	Grid substation
ICT	Interconnecting transformer
IEEE	Institute of Electrical and Electronics Engineers
IGBT	Insulated gate bipolar transistor
IGF	Index for ground fault
MATLAB	Matrix laboratory
MPPT	Maximum power point tracking
NPRL	Network protection relay
OH	Overhead
OHL	Overhead line
PV	Photovoltaic
PQ	power quality
PS	Power station
PW	Primary winding
RE	Renewable energy
SE	Solar energy
SF	Sampling frequency
SICT	Solar interconnecting transformer
SNR	Signal to noise ratio
ST	Stockwell transform
STFI	Stockwell transform-based fault index
STFT	Short time Fourier transform
SW	Secondary winding
TGI	Threshold value for IGF
TL	Transmission line
TPS	Thermal power station
UG	Underground
UGC	Underground cable
VSC	Voltage source converter
WDF	Wigner distribution function
WDFI	Wigner distribution function-based fault index

References

1. Mahela, O.P.; Gupta, N.; Khosravy, M.; Patel, N. Comprehensive Overview of Low Voltage Ride Through Methods of Grid Integrated Wind Generator. *IEEE Access* **2019**, *7*, 99299–99326. [CrossRef]
2. Telukunta, V.; Pradhan, J.; Agrawal, A.; Singh, M.; Srivani, S.G. Protection challenges under bulk penetration of renewable energy resources in power systems: A review. *CSEE J. Power Energy Syst.* **2017**, *3*, 365–379. [CrossRef]
3. Ray, P.K.; Mohanty, A.; Panigrahi, B.K.; Rout, P.K. Modified wavelet transform based fault analysis in a solar photovoltaic system. *Optik* **2018**, *168*, 754–763. [CrossRef]
4. Eissa, M.; Awadalla, M.H. Centralized protection scheme for smart grid integrated with multiple renewable resources using Internet of Energy. *Glob. Trans.* **2019**, *1*, 50–60. [CrossRef]
5. Santos, E.; Khosravy, M.; Lima, M.A.; Cerqueira, A.S.; Duque, C.A.; Yona, A. High Accuracy Power Quality Evaluation under a Colored Noisy Condition by Filter Bank ESPRIT. *Electronics* **2019**, *8*, 1259. [CrossRef]
6. Santos, E.; Khosravy, M.; Lima, M.A.; Cerqueira, A.S.; Duque, C.A. ESPRIT associated with filter bank for power-line harmonics, sub-harmonics and inter-harmonics parameters estimation. *Int. J. Electr. Power Energy Syst.* **2020**, *118*, 105731. [CrossRef]
7. Madeti, S.R.; Singh, S. A comprehensive study on different types of faults and detection techniques for solar photovoltaic system. *Solar Energy* **2017**, *158*, 161–185. [CrossRef]
8. Pothisarn, C.; Klomjit, J.; Ngaopitakkul, A.; Jettanasen, C.; Asfani, D.A.; Negara, I.M.Y. Comparison of Various Mother Wavelets for Fault Classification in Electrical Systems. *Appl. Sci.* **2020**, *10*, 1203. doi:10.3390/app10041203. [CrossRef]
9. Mahela, O.P.; Saraswat, A.; Goyal, S.K.; Jhajharia, S.; Rathore, B.; Ola, S.R. Wigner Distribution Function and Alienation Coefficient Based Transmission Line Protection Scheme. *IET Gener. Transm. Distrib.* **2020**, *14*, 1842–1853.
10. Ram Ola, S.; Saraswat, A.; Goyal, S.K.; Jhajharia, S.K.; Khan, B.; Mahela, O.P.; Haes Alhelou, H.; Siano, P. A Protection Scheme for a Power System with Solar Energy Penetration. *Appl. Sci.* **2020**, *10*, 1516. [CrossRef]
11. Ram Ola, S.; Saraswat, A.; Goyal, S.K.; Sharma, V.; Khan, B.; Mahela, O.P.; Haes Alhelou, H.; Siano, P. Alienation Coefficient and Wigner Distribution Function Based Protection Scheme for Hybrid Power System Network with Renewable Energy Penetration. *Energies* **2020**, *13*, 1120. [CrossRef]
12. Harrou, F.; Taghezouit, B.; Sun, Y. Robust and flexible strategy for fault detection in grid-connected photovoltaic systems. *Energy Convers. Manag.* **2019**, *180*, 1153–1166. [CrossRef]
13. Madeti, S.R.; Singh, S. Online modular level fault detection algorithm for grid-tied and off-grid PV systems. *Solar Energy* **2017**, *157*, 349–364. [CrossRef]
14. Manohar, M.; Koley, E.; Ghosh, S.; Mohanta, D.K.; Bansal, R. Spatio-temporal information based protection scheme for PV integrated microgrid under solar irradiance intermittency using deep convolutional neural network. *Int. J. Electr. Power Energy Syst.* **2020**, *116*, 105576. [CrossRef]
15. Suman, T.; Mahela, O.P.; Ola, S.R. Detection of transmission line faults in the presence of solar PV generation using discrete wavelet. In Proceedings of the 2016 IEEE 7th Power India International Conference (PIICON), Bikaner, India, 25–27 November 2016; pp. 1–6. [CrossRef]
16. Thukral, S.; Mahela, O.P.; Kumar, B. Detection of transmission line faults in the presence of solar PV system using stockwell's transform. In Proceedings of the 2016 IEEE 7th Power India International Conference (PIICON), Bikaner, India, 25–27 November 2016; pp. 1–6. [CrossRef]
17. Mahela, O.P.; Shaik, A.G. Recognition of power quality disturbances using S-transform based ruled decision tree and fuzzy C-means clustering classifiers. *Appl. Soft Comput.* **2017**, *59*, 243–257. [CrossRef]
18. Stockwell, R.G.; Mansinha, L.; Lowe, R.P. Localization of the complex spectrum: The S transform. *IEEE Trans. Signal Process.* **1996**, *44*, 998–1001. [CrossRef]
19. Lee, I.W.C.; Dash, P.K. S-transform-based intelligent system for classification of power quality disturbance signals. *IEEE Trans. Ind. Electron.* **2003**, *50*, 800–805. [CrossRef]
20. Mahela, O.P.; Khan, B.; Alhelou, H.H.; Tanwar, S. Assessment of power quality in the utility grid integrated with wind energy generation. *IET Power Electron.* **2020**. [CrossRef]
21. Cheng, J.Y.; Huang, S.J.; Hsieh, C.T. Application of Gabor–Wigner transform to inspect high-impedance fault-generated signals. *Int. J. Electr. Power Energy Syst.* **2015**, *73*, 192–199. [CrossRef]

22. Khan, N.A.; Taj, I.A.; Jaffri, M.N.; Ijaz, S. Cross-term elimination in Wigner distribution based on 2D signal processing techniques. *Signal Process.* **2011**, *91*, 590–599. [CrossRef]
23. Kersting, W.H. Radial distribution test feeders. *IEEE Trans. Power Syst.* **1991**, *6*, 975–985. [CrossRef]
24. Kersting, W. Radial distribution test feeders. In Proceedings of the 2001 IEEE Power Engineering Society Winter Meeting. Conference Proceedings (Cat. No.01CH37194), Columbus, OH, USA, 28 January–1 February 2001; IEEE: Piscataway, NJ, USA, 2001; Volume 2, pp. 908–912. [CrossRef]
25. Shaik, A.G.; Mahela, O.P. Power quality assessment and event detection in hybrid power system. *Electr. Power Syst. Res.* **2018**, *161*, 26–44. [CrossRef]
26. Mahela, O.P.; Khan, B.; Haes Alhelou, H.; Siano, P. Power Quality Assessment and Event Detection in Distribution Network with Wind Energy Penetration Using Stockwell Transform and Fuzzy Clustering. *IEEE Trans. Ind. Inform.* **2020**, 1. [CrossRef]
27. Alrahim Shannan, N.M.A.; Yahaya, N.Z.; Singh, B. Single-diode model and two-diode model of PV modules: A comparison. In Proceedings of the 2013 IEEE International Conference on Control System, Computing and Engineering, Mindeb, Malaysia, 29 November–1 December 2013; pp. 210–214.
28. Abdulal, F.; Anani, N.; Bowring, N. Comparative modelling and parameter extraction of a single- and two-diode model of a solar cell. In Proceedings of the 2014 9th International Symposium on Communication Systems, Networks Digital Sign (CSNDSP), Manchester, UK, 23–25 July 2014; pp. 856–860.
29. Mahela, O.P.; Shaik, A.G. Comprehensive overview of grid interfaced solar photovoltaic systems. *Renew. Sustain. Energy Rev.* **2017**, *68*, 316–332. [CrossRef]
30. Mahela, O.P.; Shaik, A.G. Power quality recognition in distribution system with solar energy penetration using S-transform and Fuzzy C-means clustering. *Renew. Energy* **2017**, *106*, 37–51. [CrossRef]
31. RVPN. Rajasthan Rajya Vidyut Prasaran Nigam Ltd. Available online: https://energy.rajasthan.gov.in/content/raj/energy-department/rajasthan-rajya-vidyut-prasaran-limited/en/about-us/power-map.html (accessed on 7 June 2020).